JOURNAL OF SOLID STATE CHEMISTRY **139,** 373–387 (1998)
ARTICLE NO. SC987861

Structure and Vibrational Spectrum of β-$Cs_3(HSO_4)_2[H_{2-x}(P_{1-x}, S_x)O_4]$ ($x \sim 0.5$), a New Superprotonic Conductor, and a Comparison with α-$Cs_3(HSO_4)_2(H_2PO_4)$

Sossina M. Haile[1]

Materials Science, 138-78, California Institute of Technology, Pasadena, California 91125

and

Pamela M. Calkins and Dane Boysen

Materials Science and Engineering, University of Washington, Seattle, Washington 98195

Received December 5, 1997; accepted April 7, 1998

The structure of the new protonic conductor, β-$Cs_3(HSO_4)_2(H_{2-x}(P_{1-x}, S_x)O_4)$ (with a superprotonic transition at 125°C), has been determined by single-crystal X-ray diffraction methods. Structural features of this and the related compound, α-$Cs_3(HSO_4)_2(H_2PO_4)$, have been further examined by Raman and IR spectroscopy. The new compound crystallizes in space group $C2/c$, contains four formula units in the unit cell, and has an x value (in the stoichiometry) of approximately 0.5. X-ray intensity data, collected at room temperature, yielded lattice parameters $a = 20.04(1)$, $b = 7.854(5)$, $c = 8.954(5)$ Å, and $\beta = 100.11(2)^\circ$ and a unit cell volume of 1387.5(14) Å^3, implying a density of 3.304 g/cm^3. Within the asymmetric unit, 10 nonhydrogen atoms and 3 hydrogen sites were located. Refinement of the X-ray data using anisotropic temperature factors for all 10 of the former yielded residuals $wR(F^2) = 0.0952$ and $R(F) = 0.0358$. The structure contains alternating zig-zig chains of anion tetrahedra and cesium ions, in a manner similar to that found in α-$Cs_3(HSO_4)_2(H_2PO_4)$ and in $CsHSO_4$-II. The structure is unique, however, in that P and S occupy the same crystallographic position, and there is, accordingly, a variable H content and a partially occupied hydrogen bond. Broader peaks in the Raman spectrum of β-$Cs_3(HSO_4)_2(H_{2-x}(P_{1-x}S_x)O_4)$ support the assumption of greater structural disorder in this compound than in α-$Cs_3(HSO_4)_2(H_2PO_4)$.

INTRODUCTION

Many solid acid sulfates and selenates undergo superprotonic phase transitions at elevated temperatures. These include $CsHSO_4$ (1), $Rb_3H(SeO_4)_3$ (2), and $Cs_5H_3(SeO_4)_4 \cdot xH_2O$ (3), and their deuterated analogs. Recently, we reported that such transitions also occur in compounds containing both SO_4 and PO_4 groups (4), thereby introducing a new class of compounds within the broad family of low-temperature proton conductors. In the present work, we describe in detail the structure of β-$Cs_3(HSO_4)_2(H_{2-x}(P_{1-x}, S_x)O_4$, the newest member of the sulfate–phosphate class of protonic conductors, as determined by X-ray diffraction. The compound undergoes a superprotonic transition at 125°C, at which the conductivity jumps from 7.9×10^{-5} to $1.3 \times 10^{-2}\,\Omega^{-1}\mathrm{cm}^{-1}$; a complete discussion of the electrical and thermal properties has been reported elsewhere (5).

EXPERIMENTAL

Synthesis

Crystals of β-$Cs_3(HSO_4)_2(H_{2-x}(P_{1-x}, S_x)O_4)$ were grown from aqueous solutions containing Cs_2CO_3, H_2SO_4, and H_3PO_4 in molar ratios of Cs : S : P of 1 : 0.8 : 0.2, as reported earlier (5). Slow evaporation of water under ambient conditions yielded plate-like crystals up to 3×5 mm in area after 5 to 7 days. Crystals grown more quickly often contained fluid inclusions that subsequently transformed into polycrystalline material. In addition, large quantities of crystalline powder of β-$Cs_3(HSO_4)_2(H_{2-x}(P_{1-x}, S_x)O_4)$ (for subsequent chemical analysis) were obtained by heating aqueous solutions of the carbonate, sulfate, and phosphate in which the molar ratio of Cs : S : P was 1 : 0.85 : 0.15 and rapidly cooling the solution to ~25°C. The identity of the crystalline precipitate that formed was confirmed by comparing its experimentally measured X-ray powder diffraction pattern with that calculated on the basis of the single-crystal structure determination.

[1]To whom all correspondence should be addressed.

0022-4596/98 $25.00

Composition Determination

The composition of the single crystals was determined by energy dispersive spectroscopy (electron microprobe) and that of the crystalline powder via bulk chemical analytical means. Samples for microprobe analysis were mounted in an epoxy resin, polished, and then sputter-coated with gold to obtain a conductive surface. Characteristic peak intensities were measured with a JEOL Superprobe 733 and converted into mass percent using the Tracor Northern analytical software (6). The compounds $CsHSO_4$, CsH_2PO_4, and α-$Cs_3(HSO_4)_2(H_2PO_4)$ served as standards. The sulfate content in the crystalline powder was determined by gravimetric measurement of $BaSO_4$, after dissolution of the sample in water and reaction with $BaCl_2$, as outlined in Christian (7).

The microprobe data, collected from two separate crystals, at three and five positions, respectively, indicated that the mole ratio of Cs : (P + S) was 1.01(2) and that of S : P was 4.2(3). This implies a value of x in β-$Cs_3(HSO_4)_2(H_{2-x}(P_{1-x}, S_x)O_4)$ of 0.42. Furthermore, the range in values in the ratio of S : P was much greater than that in the ratio of Cs : (S + P) suggesting, at first, that the composition was rather inhomogeneous. However, microprobe analysis of $Cs_5(HSO_4)_3(H_2PO_4)_2$ (8, 9), a compound in which the P : S ratio is fixed by the fact that P and S occupy distinct sites, showed a similar variation in the measured P : S values and a similar apparent deficiency in sulfur. Hence, the value of x in the single crystals is probably 0.5. The mean molar content of SO_4 in crystalline powder of β-$Cs_3(HSO_4)_2(H_{2-x}(P_{1-x}S_x)O_4)$ was found to be 2.46(5), which is within one standard deviation of the value expected for $x = 0.5$, directly indicating, in this case, a stoichiometry of $Cs_3(HSO_4)_2(H_{1.5}(P_{0.5}, S_{0.5})O_4)$.

Diffraction Data Collection

Full details of the crystal data, data collection procedure, and final refinement parameters are provided in Table 1. X-ray data were collected at room temperature, assuming a primitive unit cell. Analysis of the systematic absences subsequently showed the lattice to be C-centered.

Optical Spectroscopy

Infrared and Raman spectra were acquired at room temperature using a Nicolet System 800 FTIR spectrometer over the wavenumber range 3600 to 500 cm^{-1} and a Nicolet 950 Raman unit over the range 3600 to 300 cm^{-1}, respectively. Prior to data collection, ground powder samples were placed under vacuum at ambient temperatures for approximately 30 min to remove surface-adsorbed water. Powdered samples were used for acquiring Raman data, whereas samples for IR data collection were mixed with KBr and pressed into pellets.

TABLE 1

Crystal Data, Data Collection Parameters, Data Refinement Parameters, and Other Experimental Details for the Structure Determination and Refinement of β-$Cs_3(HSO_4)_2(H_{2-x}(P_{1-x}S_x)O_4)$

Crystal data	
Compound name	β-$Cs_3(HSO_4)_2(H_{2-x}(P_{1-x}S_x)O_4)$
Formula	$Cs_3S_{2+x}P_{1-x}O_{12}H_{4-x}$, $x \sim 0.5$
Crystal system	Monoclinic
Space group	$C2/c$
Unit cell dimensions	$a = 20.04(1)$ Å $b = 7.854(5)$ Å $c = 8.954(5)$ Å $\beta = 100.11(2)^\circ$
Unit cell volume	1387.5(14) $Å^3$
Formula weight	689.85 au
Z	4
Density (calculated)	3.304 mg m^{-3}
Absorption coefficient	7.87 mm^{-1}
Crystal size	$0.10 \times 0.15 \times 0.20$ mm^3
Crystal shape	Irregular
Crystal habit (forms)	Irregular
Crystal color	Colorless
Crystal mounted	On glass fiber with epoxy
No. of reflections for cell measurement	13 $4.9^\circ < \Theta < 10.2^\circ$
Data collection	
Temperature	293(2) K
Radiation	X-ray, Mo$K\alpha$
Wavelength	0.71073 Å
Instrument	Crystal logic diffractometer
Data collection method	Θ–2Θ scan
$F(000)$	1248.0
Absorption correction method	Empirical, Ψ scan
Maximum and minimum transimission factors	0.82 and 1.00
Theta range for data collection	2.01–27.50
Index ranges	$0 \le h \le 23$, $0 \le k \le 9$, $-10 \le l \le 10$
Reflections collected	2607 (assuming C centering)
Independent reflections	1121 ($R_{int} = 0.0216$)
Significant reflections	950 ($I > -2\sigma$)
Standards	[(−2,2,1), (−4, −2, −1), (0,2, −3)]
Deviation of standards from initial value	Stable
Decay correction	None applied
Refinement	
Refinement method	F^2
$wR[F^2 > 2\sigma(F^2)]$	0.0840
$wR(F^2)$	0.0952
$R[F > 4\sigma(F)]$	0.0358
Goodness-of-fit, S, on F^2	1.116
No. of reflections used in refinement	1121
No. of refined parameters	84
Weighting scheme	$w = [\sigma^2(F_0^2) + (0.0106*P)^2 + 7.08*P]^{-1}$ where $P = (1/3)*(\mathrm{Max}(F_0^2, 0) + 2*F_c^2)$
(Δ/σ) max/mean	0.268, 0.038
Fourier differences peaks max/min	1.36/ −1.58e $Å^{-3}$

TABLE 1—*Continued*

Refinement	
Anisotropic thermal parameters	All nonhydrogen atoms
Extinction method	Sheldrick (1992)
Extinction coefficient	0.0107(14)
Sources of atomic scattering factors	Cromer and Waber (12)
Treatment of H atom	Not refined from X-ray data: positions as determined from a preliminary refinement of neutron data are reported
Computer programs	
Structure solution	SHELXS (13)
Structure refinement	SHELXL (14)
Structure depiction	ATOMS from Shape Software
Powder analysis	JADE from Materials Data, Inc.

TABLE 2
Atomic Coordinates and Equivalent Isotropic Displacement Parameters ($Å^2 \times 10^2$) for β-$Cs_3(HSO_4)_2(H_{2-x}(P_{1-x}S_x)O_4$

Atom	Site	x	y	z	U(eq)
Cs(1)	4*e*	$\frac{1}{2}$	0.40247(8)	$\frac{1}{4}$	4.01(3)
Cs(2)	8*f*	0.32339(3)	0.13433(7)	0.38214(7)	4.94(3)
(P, S)[a]	4*e*	$\frac{1}{2}$	0.9061(3)	$\frac{1}{4}$	3.78(5)
S	8*f*	0.15878(9)	0.1286(2)	0.0703(2)	3.03(6)
$O(1)_{A/D}$	8*f*	0.5252(3)	0.0208(6)	0.1351(5)	3.86(12)
$O(2)_A$	8*f*	0.4425(3)	0.7994(7)	0.1710(6)	4.60(14)
$O(3)_D$	8*f*	0.1658(3)	0.7719(7)	0.7191(6)	4.78(14)
O(4)	8*f*	0.1026(3)	0.9871(8)	0.5600(7)	5.9(2)
$O(5)_{A*}$	8*f*	0.2215(3)	0.9623(9)	0.5781(8)	7.4(2)
$O(6)_{D*}$	8*f*	0.1465(4)	0.7484(8)	0.4478(7)	6.7(2)

Note. U(eq) is defined as one-third of the trace of the orthogonalized U_{ij} tensor. The subscripts D, A, and A/D indicate donor, acceptor, and mixed donor–acceptor oxygen atoms, respectively, in a hydrogen bond. An asterisk indicates that the oxygen atom only weakly participates in a hydrogen bond (see text for further explanation).

[a]Occupancy fixed at (0.5P, 0.5S).

RESULTS

Structure Determination and Refinement

On the basis of systematic absences ($h + k = 2n + l$ absent, and $l = 2n + 1$ absent for $h01$ peaks), the space group $C2/c$ was selected as the starting point for the solution of the structure and later proved to be the most appropriate. The structure was solved by first locating the Cs and X atom sites, where X = P or S, from direct methods. The O atom sites were identified from subsequent Fourier difference maps. From these data alone, it was impossible to directly determine which of the X atoms should be sulfur and which should be phosphorus. However, on the basis of the chemical analysis, and the similarity of the structure of β-$Cs_3(HSO_4)_2(H_{2-x}(P_{1-x}S_x)O_4)$ to that of α-$Cs_3(HSO_4)_2(H_2PO_4)$ (10), as discussed below, it was presumed that the X atom position located at an 8*f* site was occupied entirely by sulfur and that at a 4*e* site by both phosphorus and sulfur (see Table 2). More recent neutron diffraction studies (to be published shortly) have confirmed this presumption, and suggest, in agreement with the chemical analysis, that the P : S ratio at the 4*e* site is 0.5 : 0.5. The X-ray data were also unable to directly reveal the location of hydrogen atoms from Fourier difference maps. However, an examination of intertetrahedral oxygen–oxygen distances suggested that three hydrogen sites existed, the first linking O(1) and O(1′), the second linking O(2) and O(3), and the third weakly linking O(5) and O(6). At the third site, partial occupancy was presumed both because of the long O(5)–O(6) distance, 3.163(10) Å, and because full occupancy would have provided more hydrogen than was expected on the basis of the chemical analysis. These assumptions have also been, to a great extent, supported by the neutron studies (11).

In the latter stages of the refinement, the possibility that the structure crystallized in a lower-symmetry space group was explored, particularly because a few systematic absence violations of the C centering had been observed. Specifically, 5 of approximately 1430 peaks with indices $h + l = 2n + l$ had intensity greater than 4σ. The non-centered space groups examined were $P2/c$, $P2$, and Pc. In addition, the non-centrosymmetric space group Cc was examined. Pseudosymmetry-related atoms were generated and refinement was carried out by either letting all parameters vary independently or by explicitly linking the values of appropriately selected parameters. In those few cases where the refinement did not simply fail, all pseudosymmetry-related parameters (that were not explicitly linked) were correlated above the 80% level. Furthermore, in no case did the quality of the refinement, as measured by the magnitudes of the standard deviations of refined parameters and chemical reasonableness of the solution, improve. Hence, $C2/c$ was taken as the correct space group.

In the final refinement the scale factor, all atomic coordinates, and all anisotropic displacement parameters were varied. A refined extinction correction was applied, but it became apparent that this correction could not adequately describe the reduction in intensity of very strong peaks and, thus those peaks of intensity greater that 15,000 cps (106 of 2713) were omitted. The final residual obtained was $wR(F^2) = 0.0952$ (Table 1). The largest peak in the difference map was $1.36\ e\ Å^{-3}$ and the deepest hole $-1.58\ e\ Å^{-3}$. While the refinement was carried out by minimizing a weighted residual based on F^2 and using all data, the value of a more conventional $R(F)$ calculated from "observed" data, $F_0 > 4\sigma(F_0)$, is provided for comparison with older literature R values. Calculated and observed F^2 have been

TABLE 3
Anisotropic Displacement Parameters ($Å^2 \times 10^2$) for β-$Cs_3(HSO_4)_2(H_{2-x}(P_{1-x}S_x)O_4$

Atom	U_{11}	U_{22}	U_{33}	U_{23}	U_{13}	U_{12}
Cs(1)	3.66(4)	3.34(4)	4.93(5)	0	0.48(3)	0
Cs(2)	3.42(4)	4.10(4)	7.05(5)	− 0.71(2)	0.25(3)	0.23(2)
(P, S)	3.74(14)	2.95(12)	2.34(12)	0	0.38(10)	0
S	3.39(10)	3.49(10)	4.50(12)	− 0.19(8)	0.80(9)	0.11(7)
$O(1)_{A/D}$	4.6(3)	3.9(3)	3.0(3)	− 0.2(2)	0.4(2)	− 1.5(2)
$O(2)_A$	5.3(3)	4.6(3)	3.9(3)	− 0.1(2)	0.6(3)	− 1.8(3)
$O(3)_D$	4.4(3)	5.0(3)	4.6(3)	1.4(3)	0.0(2)	− 0.6(2)
O(4)	6.0(4)	6.1(4)	5.4(3)	0.4(3)	0.6(3)	2.3(3)
$O(5)_{A^*}$	5.5(4)	8.5(5)	7.6(5)	3.1(4)	− 0.3(3)	− 2.8(4)
$O(6)_{D^*}$	9.9(5)	5.7(4)	4.1(3)	− 1.1(3)	0.4(3)	1.5(4)

Note. The anisotropic displacement factor exponent takes the form $-2\pi^2[h^2a^{*2}U_{11} + \cdots + 2hka^*b^*U_{12}]$.

TABLE 4
Interatomic Distances and Angles in the Coordination Polyhedra of β-$Cs_3(HSO_4)_2(H_{2-x}(P_{1-x}S_x)O_4)$

Cs(1)–	Distance, Å	Cs(2)–	Distance, Å	
O(4)\$1[a]	3.017(6)	O(1)\$5	3.193(5)	
O(4)\$2	3.017(6)	O(5)\$7	3.195(7)	
O(4)\$3	3.220(6)	O(5)\$6	3.214(6)	
O(4)\$4	3.220(6)	O(2)\$8	3.238(6)	
O(1)	3.237(5)	O(6)\$4	3.243(6)	
O(1)\$5	3.237(5)	O(3)\$7	3.321(6)	
O(2)\$5	3.356(6)	O(4)\$2	3.323(7)	
O(2)	3.356(6)	O(5)\$2	3.329(8)	
O(6)\$3	3.376(7)	O(3)\$9	3.334(6)	
O(6)\$4	3.376(7)	O(6)\$9	3.376(7)	
		O(3)\$10	3.700(6)	
P, S–	Distance, Å		Angles, °	
$O(2)_A$	1.499 (5)			
$O(2)_A$ \$5	1.499 (5)	112.0 (5)		
$O(1)_{A/D}$ \$11	1.519 (5)	109.4 (3)	109.3 (3)	
$O(1)_{A/D}$ \$12	1.519 (5)	109.3 (3)	109.4 (3)	107.2 (4)
	S, P–	O(2)	O(2)\$5	O(1)\$11
O–O	Distances, Å			
O(2)\$5	2.485 (11)			
O(1)\$11	2.462 (7)	2.463 (7)		
O(1)\$12	2.463 (7)	2.462 (7)	2.445 (9)	
	O(2)	O(2)\$5	O(1)\$11	
S–	Distance, Å		Angles, °	
$O(5)_{A^*}$ \$7	1.437 (6)			
O(4)\$7	1.438 (6)	111.0 (5)		
$O(6)_{D^*}$ \$7	1.450 (6)	113.5 (5)	110.2 (4)	
$O(3)_A$ \$7	1.530 (6)	105.4 (4)	109.3 (3)	107.2 (4)
	S(1)–	O(5)\$7	O(4)\$7	O(6)\$7
O–O	Distances, Å			
O(4)\$7	2.368 (10)			
O(6)\$7	2.414 (10)	2.369 (8)		
O(3)\$7	2.360 (8)	2.421 (8)	2.399 (8)	
	O(5)\$7	O(4)\$7	O(6)\$7	

[a] Symmetry codes:

\$1	$x+\frac{1}{2}, -y+\frac{3}{2}, z-\frac{1}{2}$	\$2	$-x+\frac{1}{2}, -y+\frac{3}{2}, -z+1$
\$3	$x+\frac{1}{2}, y-\frac{1}{2}, z$	\$4	$-x+\frac{1}{2}, y-\frac{1}{2}, -z+\frac{1}{2}$
\$5	$-x+1, y, -z+\frac{1}{2}$	\$6	$x, y-1, z$
\$7	$x, -y+1, z-\frac{1}{2}$	\$8	$x, -y+1, z+\frac{1}{2}$
\$9	$-x+\frac{1}{2}, -y+\frac{1}{2}, -z+1$	\$10	$-x+\frac{1}{2}, y-\frac{1}{2}, -z+\frac{3}{2}$
\$11	$-x+1, y+1, -z+\frac{1}{2}$	\$12	$x, y+1, z$

deposited. The atomic coordinates and thermal parameters are given in Tables 2 and 3, respectively. Interatomic distances in the cation coordination polyhedra are reported in Table 4. Hydrogen bond lengths and some preliminary geometric details obtained from the neutron studies are provided in Table 5.

Optical Spectroscopy

The low-frequency IR and Raman spectra of β-$Cs_3(HSO_4)_2(H_{2-x}(P_{1-x}S_x)O_4)$ and of α-$Cs_3(HSO_4)_2(H_2PO_4)$ are shown in Fig. 1. Peak positions in the Raman spectra are indicated in the accompanying fitted plots (Fig. 2; see also Table 8 below). It is apparent, even before any assignment of peaks to specific motions is made, that the peaks in the Raman spectrum of β-$Cs_3(HSO_4)_2(H_{2-x}(P_{1-x}S_x)O_4)$ are significantly broader than those of α-$Cs_3(HSO_4)_2(H_2PO_4)$, suggesting an overall greater degree of disorder in the former. The high-frequency spectra (both IR and Raman) were generally featureless, with the exception of three very broad peaks, in the vicinity of 2700, 2300, and 1700 cm^{-1} for both compounds. Specifically, these were observed for β-$Cs_3(HSO_4)_2(H_{2-x}(P_{1-x}S_x)O_4)$ at 2820, 2320, and 1700 cm^{-1} by Raman spectroscopy and at 2850, 2300, and 1650 cm^{-1} by IR. For α-$Cs_3(HSO_4)_2(H_2PO_4)$ the peaks appeared at 2870, 2480, and 1640 cm^{-1} by Raman methods and at 2900, 2300, and 1650 cm^{-1} by IR.

DISCUSSION

Polyhedral Coordination

The compound β-$Cs_3(HSO_4)_2(H_{2-x}(P_{1-x}S_x)O_4)$ contains 10 independent, nonhydrogen atom sites in the asymmetric unit. The two crystallographically independent Cs atoms are coordinated by 10 and 11 oxygen atoms, respectively. The observed coordination numbers and average Cs–O distance, 3.28(14) Å, are consistent with typical values for Cs (15). The S and P atoms are tetrahedrally coordinated by oxygen. The *X*–O distances determined, with an average of 1.49(4) Å, are also quite reasonable. Differences between *X*–O lengths are discussed below in the

TABLE 5
Atomic Coordinates of Protons in β-$Cs_3(HSO_4)_2(H_{2-x}(P_{1-x}S_x)O_4)$ as Determined from a Preliminary Refinement of Neutron Data (full details to be published shortly) and the Geometry of the Associated Hydrogen Bonds

Atom	x	y	z	O neighbors	Site symmetry	d(O···O) (Å)	d(O–H) (Å)	d(O···H) (Å)	∠OHO (°)
H(1)[a]	0.5	0	0	$O(1)_{A/D}$–$O(1)_{A/D}$\$1[b]	$\bar{1}$	2.474 (9)	1.237	(1.237)	180
H(2)	0.1157(2)	0.7435(4)	0.7603(4)	$O(2)_D$–$O(3)_A$\$2	1	2.597 (8)	1.151	1.450	173.1
H(3)[c]	0.2072(2)	0.6906(11)	0.4490(9)	$O(5)_{A*}$–$O(6)_{D*}$\$2	1	3.163 (10)	1.296	1.914	159.8

[a] Proton probably displaced from the center of symmetry.
[b] Symmetry codes: \$1: $-x+1, -y, -z$; \$2: $-x+\frac{1}{2}, -y+\frac{3}{2}, -z+1$.
[c] Site occupancy ≈ 0.25.

context of the hydrogen bonds formed between the oxygen atoms of neighboring tetrahedral groups. The thermal ellipsoids obtained (Fig. 3) show the Cs, S, and P atoms to exhibit rather isotropic thermal displacements and the oxygen atoms to undergo the greatest thermal displacements in a direction perpendicular to the X–O bond, as would be expected in such a compound.

Hydrogen Bonds

It is well known that X–OH distances are, in general, longer than X–O distances, and that X–OH distances increase as the strength of the hydrogen bond, O–H···O increases, that is, as O···O decreases. Moreover, it is also rather well-established that in response to increases in X–OH bond lengths, the remaining X–O bonds of an XO_4 group tend to shorten. In our investigation of the structures of α-$Cs_3(HSO_4)_2(H_2PO_4)$ and $Cs_5(HSO_4)_3(H_2PO_4)_2$ use of correlations between X–OH, X–O, and O···O distances proved a powerful tool for identifying donor (O_D), acceptor (O_A), and non-hydrogen-bonded oxygen atoms, and for distinguishing between single- and double-minimum potential wells. For brevity, we refer to the latter type of hydrogen bond as "disordered." In Fig. 4 the linear regression curves

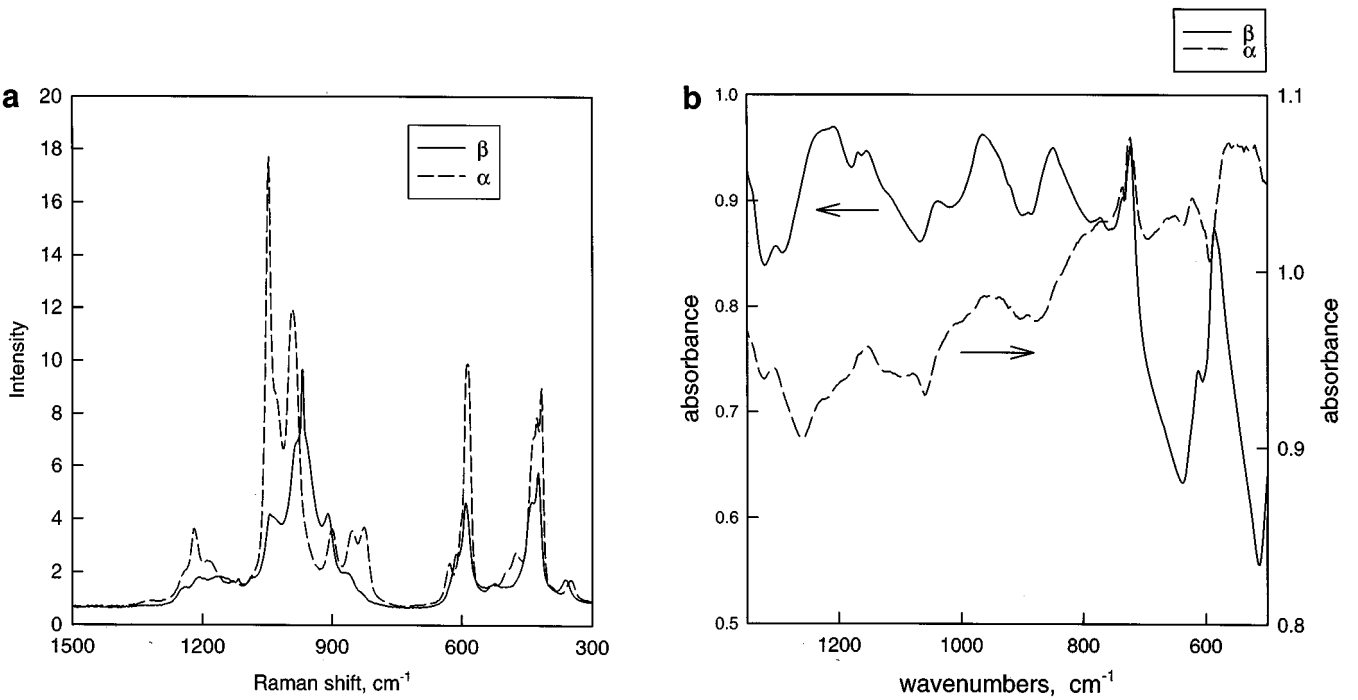

FIG. 1. Optical spectra obtained for β-$Cs_3(HSO_4)_2(H_{2-x}(P_{1-x}S_x)O_4)$ and α-$CS_3(HSO_4)_2(H_2PO_4)$. (a) Raman spectra. (b) Infrared spectra.

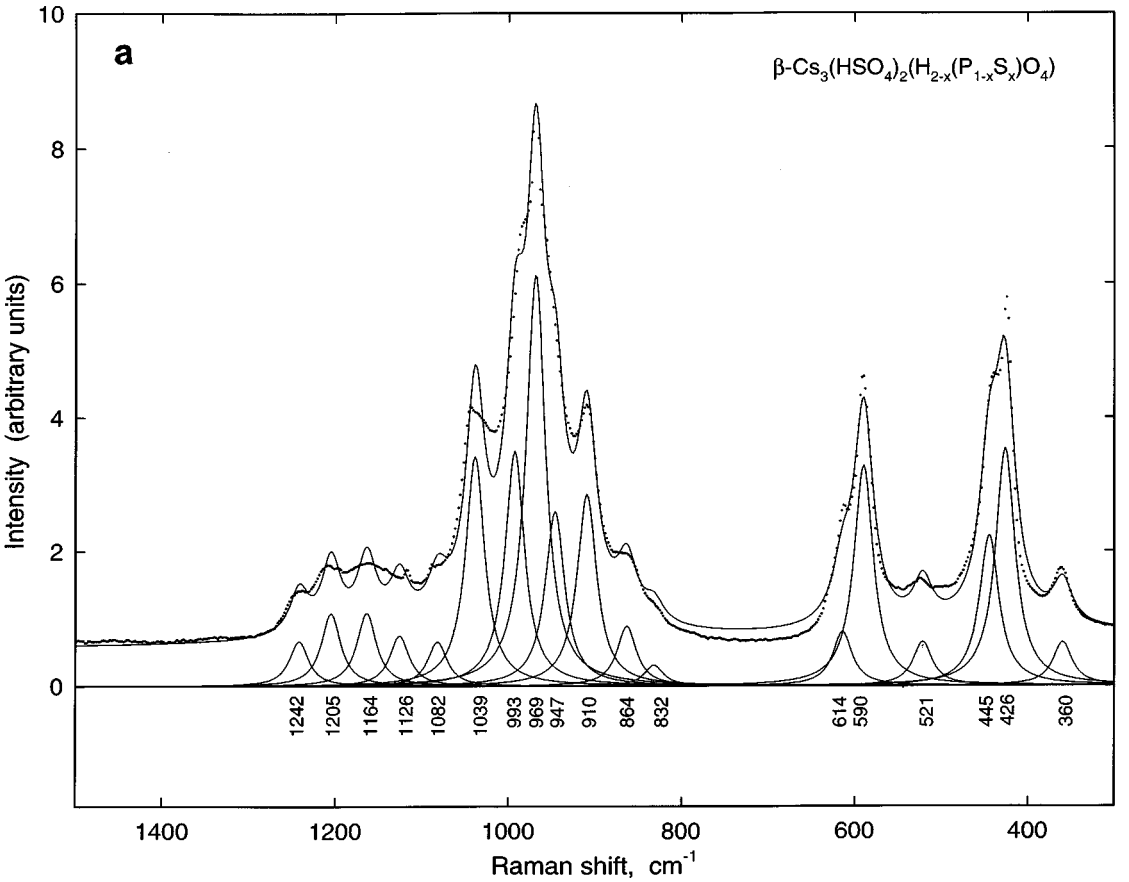

FIG. 2. Locations of fitted peaks to the Raman spectra of (a) β-$Cs_3(HSO_4)_2(H_{2-x}(P_{1-x}S_x)O_4)$—Lorentzian peaks with FWHM of 15 cm^{-1}, and (b) α-$CS_3(HSO_4)_2(H_2PO_4)$—Pearson VII peaks with FWHM of 27 cm^{-1}.

of X–O(H) versus O···O are compared with the distances obtained in β-$Cs_3(HSO_4)_2(H_{2-x}(S_xP_{1-x})O_4)$. The data for P–O(H) refer to a phosphate group in which two oxygen atoms serve as donors in an H bond (H_2PO_4 group) and were taken from Ichikawa (16); those for S–O(H) refer to a sulfate group containing only one donor oxygen atom (HSO_4) and were taken from Haile and Calkins (8).

Data point (a) of Fig. 4, representing the symmetric bond about H(1), shows that the (P, S)–O(1) bonds are elongated relative to typical P–O and S–O bonds, and confirms that the O(1) atoms are involved in forming hydrogen bonds. The O(1)···O(1) distance, 2.474(9) Å, is at the lower limit of observed double-minimum symmetric bond lengths (17). The combination of O···O and X–O lengths is comparable to that of the disordered bond in CsH_2PO_4, 2.472(7) and 1.529(4) Å, respectively (18), and in $K_3H(SO_4)_2$, 2.493(1) and 1.534(1) Å, respectively (19). These observations suggest that the bond formed by H(1) in β-$Cs_3(HSO_4)_2(H_{2-x}(P_{1-x}S_x)O_4)$ should also be disordered, with the configuration $O(1)_{A/D}$–$H(1)_{1/2}$–$H(1)_{1/2}$–$O(1')_{A/D}$. Examining the X–O bond distances associated with the H(2) bond, the greater S–O(3) length than (P, S)–O(2) indicates that O(3) should be the donor atom and O(2) the acceptor. However, the difference in lengths is not as large as normally observed, and suggests that H(2) may, in fact, reside in an asymmetric double-minimum potential. The S–O distances for the remaining oxygen atoms, points (d), (e), and (f) of Fig. 4, lie almost directly on the linear regression curve for a sulfate group that has one donor oxygen atom, further indicating that O(3) is the single donor oxygen atom in the SO_4 group. As stated earlier, the third proton, H(3), resides between two oxygen atoms, O(5) and O(6), that are rather far apart, 3.160 Å. While it would be meaningless to extend the linear regression curves of Fig. 4 to this value, as such long hydrogen bonds are rarely observed, it can be concluded that the bond between O(5) and O(6) is rather weak. Weak hydrogen bonds are normally accompanied by short O_D–H distances and imply long X–O_D distances. In this case, however, neither S–O(5) nor S–O(6) appears affected by the presence

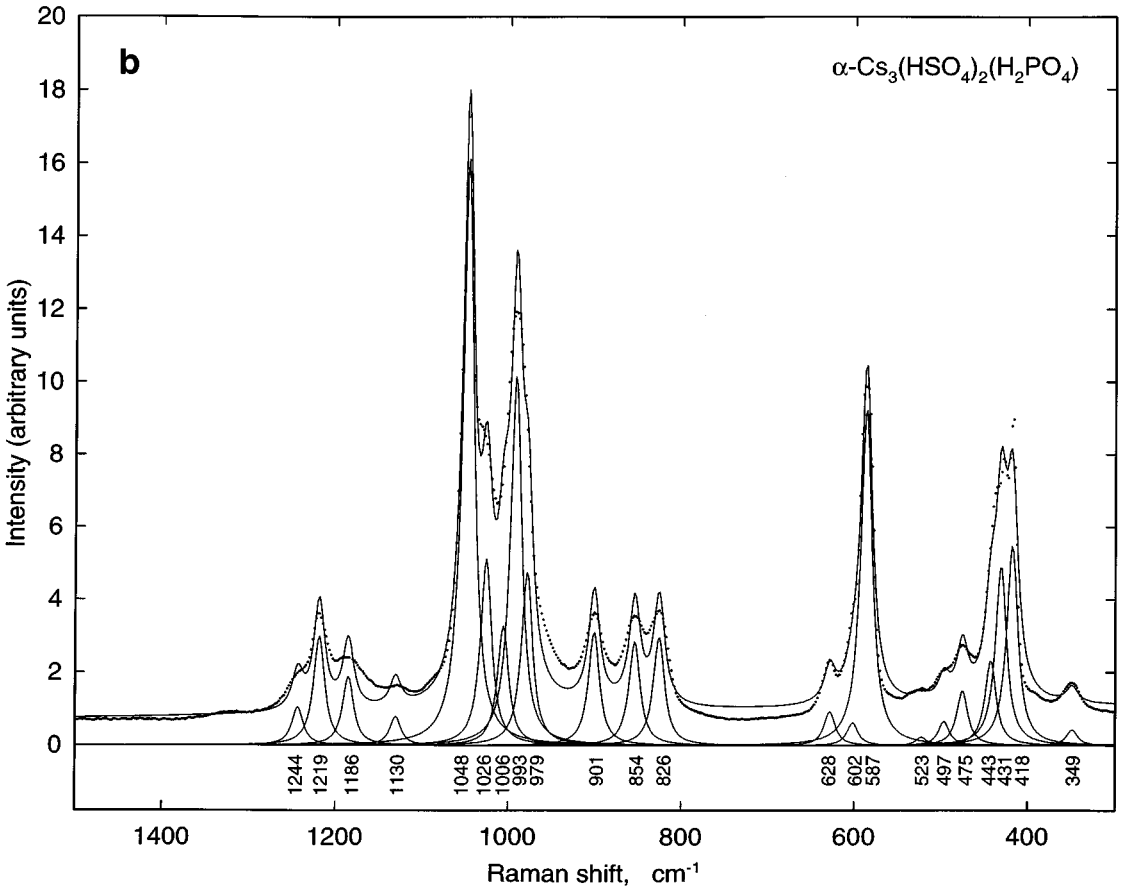

FIG. 2—*Continued*

of the proton. The simultaneous observation of a long O···O bond and normal *X*–O distances can be explained by a low occupancy at the H(3) site, as was already proposed for stoichiometric reasons.

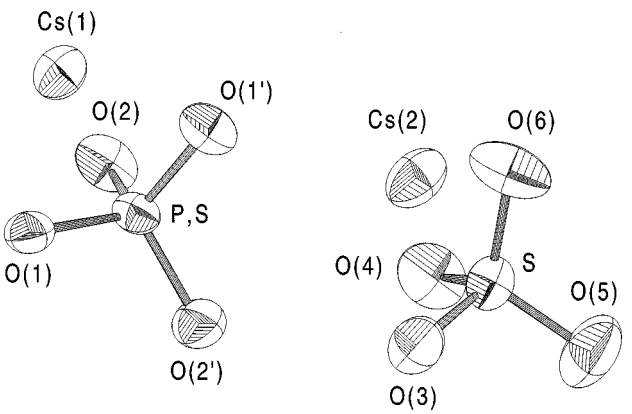

FIG. 3. Thermal ellipsoid representation of the structure of β-$Cs_3(HSO_4)_2(H_{2-x}(P_{1-x}S_x)O_4)$ with an electron probability of 50%.

Polyhedral Connectivity and Comparisons to Similar Structures

The arrangement of Cs cations and of XO_4 anions in β-$Cs_3(HSO_4)_2(H_{2-x}(P_{1-x}S_x)O_4)$ is very similar to that found in α-$Cs_3(HSO_4)_2(H_2PO_4)$ (10), in $CsHSO_4$-II (mid-temperature phase) (20) and in the $CsHSO_4$-like region of $Cs_5(HSO_4)_3(H_2PO_4)_2$ (8). A preliminary discussion of the structural relationship between the first two sulfate–phosphates has been provided in Haile *et al.* (5), and that between α-$Cs_3(HSO_4)_2(H_2PO_4)$ and $CsHSO_4$-II has been reported in Haile *et al.* (10). We present here a more detailed comparison of β-$Cs_3(HSO_4)_2(H_{2-x}(P_{1-x}S_x)O_4)$ with its closest relative, α-$Cs_3(HSO_4)_2(H_2PO_4)$. A broader examination of the structural relationships between all the compounds in this class of sulfate–phosphates is presented in Haile and Calkins (8).

Both the α-$Cs_3(HSO_4)_2(H_2PO_4)$ and β-$Cs_3(HSO_4)_2(H_{2-x}(P_{1-x}S_x)O_4)$ structures are comprised of zig-zag chains of Cs cations and of XO_4 anions that alternate with one another in a checkerboard fashion. In addition, the lattice parameters of α-$Cs_3(HSO_4)_2(H_2PO_4)$, $a = 19.546(3)$,

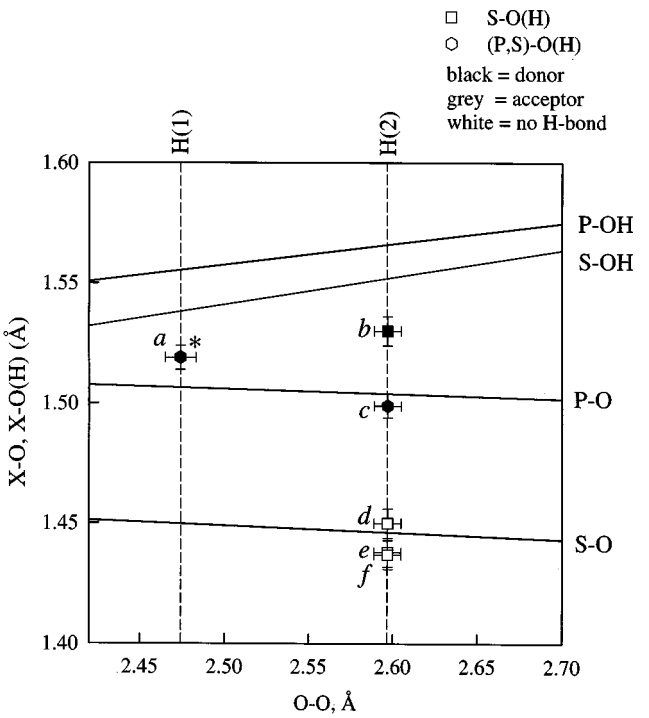

FIG. 4. The X–O versus O···O data points of β-$Cs_3(HSO_4)_2(H_{2-x}(P_{1-x}S_x)O_4)$ as compared with the linear regression curves for $SO_3(OH)$ (8) and PO_2 (16). Data points refer to the following bond distance pairs: (a) (P, S)–O(1) versus O(1)–O(1); (b) S–O(3) versus O(2)–O(3); (c) (P, S)–O(2) versus O(2)–O(3); (d) S–O(6) versus O(2)–O(3); (e) S–O(4) versus O(2)–O(3); (f) S–O(5) versus O(2)–O(3). An asterisk indicates that the oxygen atom (of X–O) serves as both donor and acceptor.

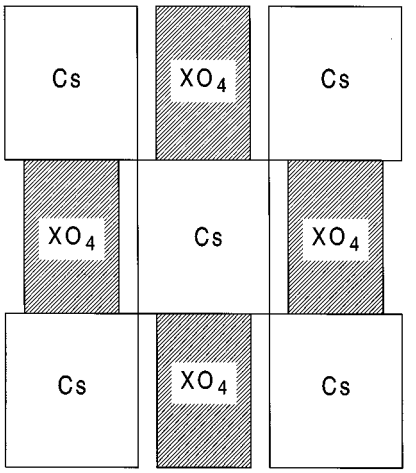

FIG. 5. Schematic depiction of the checkerboard arrangement of Cs cation and of XO_4 anion chains in β-$Cs_3(HSO_4)_2(H_{2-x}(P_{1-x}S_x)O_4)$. Chains extend out of the plane of the paper.

$b = 7.8798(10)$, $c = 9.1854(17)$ Å, and $\beta = 100.534(14)^\circ$ (10), are almost identical to those of the present compound, as are the atomic coordinates (Table 6). The former crystallizes in space group $P2_1/n$, however, in contrast to $C2/c$ for β-$Cs_3(HSO_4)_2(H_{2-x}(P_{1-x}S_x)O_4)$, and thus the asymmetric unit is twice as large. The arrangement of the two types of chains is shown schematically in projection along the direction of chain extension in Fig. 5, whereas the zig-zag nature of the chains is evident in Fig. 6. The primary differences between the α and β structures are the location and quantity of phosphorus atoms and the nature of the hydrogen bond network. In α-$Cs_3(HSO_4)_2(H_2PO_4)$ every third atom along the zig-zag XO_4 chain consists of a PO_4 group. In contrast, in β-$Cs_3(HSO_4)_2(H_{2-x}(P_{1-x}S_x)O_4)$ every third anion consists of a (P, S)O_4 group; that is, every third XO_4 group along the anion chain has a 50% probability of being either a phosphate group or a sulfate group. It is in this manner than the differences in the P : S ratio between the two compounds is accommodated.

In both compounds disordered hydrogen bonds exists between neighboring chains at the PO_4/(P, S)O_4 anion sites. Along the length of the chains, α-$Cs_3(HSO_4)_2(H_2PO_4)$ has asymmetric, fully occupied hydrogen bonds between each XO_4 group. Accordingly, PO_4 groups are saturated with respect to hydrogen bonds (all four oxygen atoms participate in hydrogen bond formation), and the linkage between atoms has the following configuration:

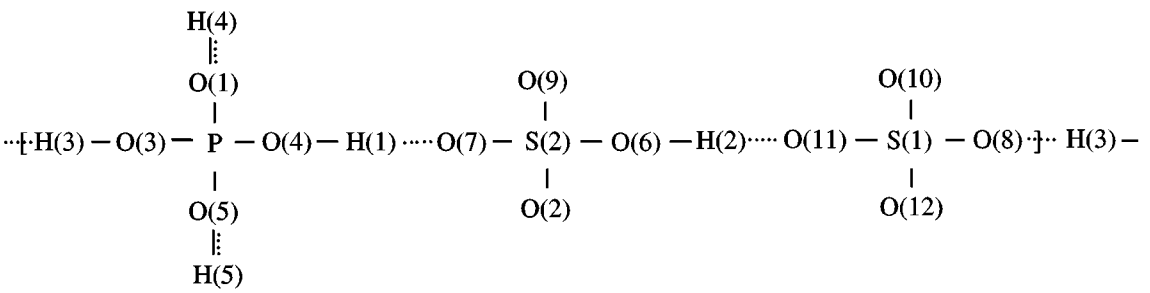

where ⋯ denote a disordered hydrogen bond between $O_{A/D}$ and H; — denotes a normal X–O bond, or one between O_D and H; and .... denotes a bond between O_A and H.

TABLE 6
Comparison of the Atomic Coordinates of β-$Cs_3(HSO_4)_2(H_{2-x}(P_{1-x}S_x)O_4)$ (present work) and α-$Cs_3(HSO_4)_2(H_2PO_4)$ (10)

β	x	y	z	U(eq)	α	x	y	z	U(eq)
Cs(1)	0.5000	0.40247(8)	0.2500	0.0401(3)	Cs(3)	0.49681(2)	0.40789(5)	0.25988(4)	0.03644(12)
Cs(2)	0.32339(3)	0.13433(7)	0.38214(7)	0.0494(3)	Cs(1)	0.31893(2)	0.13498(5)	0.40528(4)	0.03998(13)
Cs(2)$1[a]	0.32339(3)	0.86567(7)	0.88214(7)	0.0494(3)	Cs(2)	0.32727(2)	0.85447(4)	0.86607(4)	0.03707(13)
(P, S)[b]	0.5000	0.9061(3)	0.2500	0.0303(6)	P	0.49237(7)	0.9185(2)	0.24896(13)	0.0268(3)
S(1)	0.15878(9)	0.1286(2)	0.0703(2)	0.0378(5)	S(1)	0.16309(7)	0.1405(2)	0.06215(15)	0.0307(3)
S(1)$1	0.15878(9)	0.8714(2)	0.5703(2)	0.0378(5)	S(2)	0.15817(7)	0.8676(2)	0.5803(2)	0.0326(3)
$O(1)_{A/D}$	0.5252(3)	0.0208(6)	0.1351(5)	0.0386(12)	$O(1)_{A/D}$	0.5171(2)	0.0287(5)	0.1330(4)	0.0349(8)
$O(1)_{A/D}$$2	0.4748(3)	0.0208(6)	0.3649(5)	0.0386(12)	$O(5)_{A/D}$	0.4714(2)	0.0264(5)	0.3710(4)	0.0321(8)
$O(2)_A$	0.4425(3)	0.7994(7)	0.1710(6)	0.0460(14)	$O(3)_D$	0.4315(2)	0.8072(6)	0.1744(4)	0.0431(10)
$O(2)_A$$1	0.4425(3)	0.2006(7)	0.5710(6)	0.0460(14)	$O(4)_D$	0.4473(2)	0.1993(5)	0.6777(4)	0.0416(9)
$O(3)_D$	0.1658(3)	0.7719(7)	0.7191(6)	0.0478(14)	$O(7)_A$	0.1644(2)	0.7554(6)	0.7110(5)	0.0439(10)
$O(3)_D$$1	0.1658(3)	0.2281(7)	0.2191(6)	0.0478(14)	$O(8)_A$	0.1719(2)	0.2376(6)	0.2065(5)	0.0432(10)
O(4)	0.1026(3)	0.9871(8)	0.5600(7)	0.059(2)	O(9)	0.0927(2)	0.9581(6)	0.5520(5)	0.0519(12)
O(4)$3	0.6026(3)	0.4871(8)	0.5600(7)	0.059(2)	O(12)	0.6141(2)	0.4963(6)	0.5598(5)	0.0486(11)
$O(5)_{A*}$	0.2215(3)	0.9623(9)	0.5781(8)	0.074(2)	O(2)	0.2181(2)	0.9794(5)	0.5972(5)	0.0484(11)
$O(5)_{A*}$$1	0.2215(3)	0.0377(9)	0.0781(8)	0.074(2)	$O(11)_A$	0.2337(2)	0.0701(6)	0.0571(5)	0.0488(11)
$O(6)_{D*}$	0.1465(4)	0.7484(8)	0.4478(7)	0.067(2)	$O(6)_D$	0.1596(3)	0.7529(6)	0.4457(5)	0.0517(11)
$O(6)_{D*}$$3	0.6465(4)	0.2484(8)	0.4478(7)	0.067(2)	O(10)	0.6420(3)	0.2411(6)	0.4411(5)	0.0505(11)
H(1)	0.5	0	0		H(4)[c]	0.498	0.985	0.039	
H(1)$1	0.5	0	0.5		H(5)[c]	0.498	0.991	0.468	
H(2)	0.1157(2)	0.7435(4)	0.7603(4)		H(1)	0.118	0.745	0.741	
H(2)$4	0.3843(2)	0.7565(4)	0.2397(4)		H(3)	0.397	0.797	0.241	
H(3)[d]	0.2072(2)	0.6906(11)	0.4490(9)		H(2)	0.204	0.690	0.460	

Note. Coordinates of some hydrogen atoms [H(1), H(4), and H(5)] in the latter compound were in error in original work and have been corrected here.
[a] Symmetry codes: $1: x, $1-y$, $z+0.5$; $2: $1-x$, y, $-z+0.5$; $3: $x+0.5$, $y+0.5$, z; $4: $-x+0.5$, $-y+0.5$, $-z$.
[b] Site occupied by 0.5P and 0.5S.
[c] Site occupancy of 0.5, presumed to correspond to locally disordered hydrogen bonds with protons slightly displaced from center of symmetry.
[d] Site occupancy of 0.25.

In β-$Cs_3(HSO_4)_2(H_{2-x}(P_{1-x}S_x)O_4)$, similar, asymmetric, fully occupied hydrogen bonds exist between $(P,S)O_4$ and SO_4 groups, and thus the $(P,S)O_4$ anions are also saturated with respect to hydrogen bonds. Neighboring SO_4 groups, however, are linked by a pair of crystallographically equivalent hydrogen bonds with low proton occupancy (Fig. 6a), resulting in the following bond scheme:

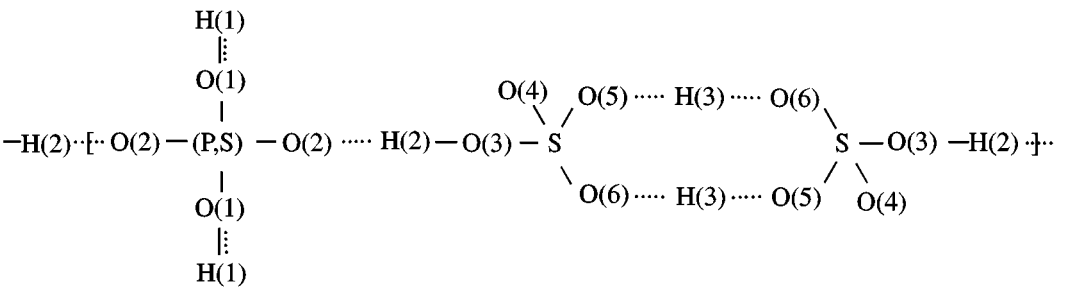

From a crystallographic perspective, cyclic dimers are formed by neighboring sulfate groups in β-$Cs_3(HSO_4)_2(H_{2-x}(P_{1-x}S_x)O_4)$ and not in α-$Cs_3(HSO_4)_2(H_2PO_4)$, because there is a center of inversion at $(\frac{1}{4}\frac{1}{4}0)$ in $C2/c$ that does not exist in $P2_1/n$ (Fig. 7). This operation causes there to be two H(3) hydrogen bonds in β-$Cs_3(HSO_4)_2(H_{2-x}(P_{1-x}S_x)O_4)$ where there is only one bond, H(2), in α-$Cs_3(HSO_4)_2(H_2PO_4)$. That is, placement of a hydrogen bond between one pair of oxygen atoms, O(5) and O(6′), linking two sulfate anions in β-$Cs_3(HSO_4)_2(H_{2-x}(P_{1-x}S_x)O_4)$ must be accompanied by the introduction of a second hydrogen bond between a related pair of oxygen atoms, O(5′) and O(6), that links the same two sulfate anions.

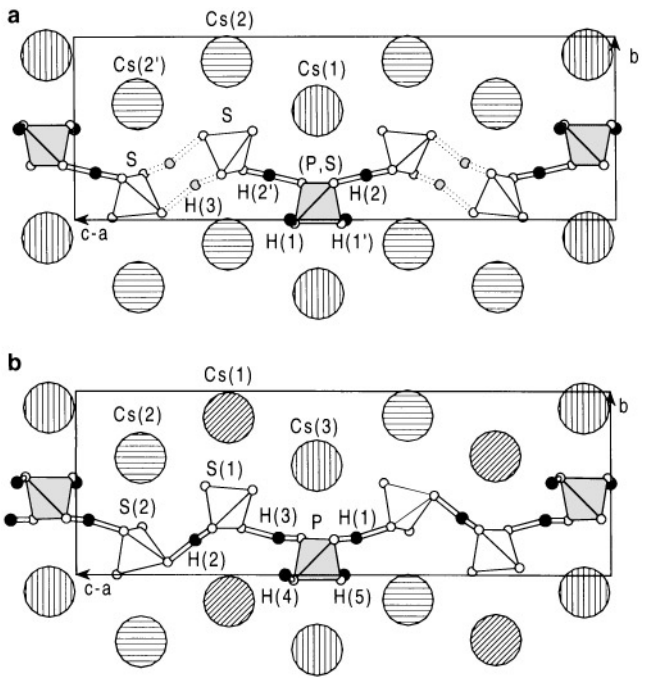

FIG. 6. Projections of the structures of (a) β-$Cs_3(HSO_4)_2(H_{2-x}(P_{1-x}S_x)O_4)$ and (b) α-$CS_3(HSO_4)_2(H_2PO_4)$ on (101) showing the zig-zag Cs cation chains and the hydrogen bonded XO_4 anion chains.

From a chemical perspective, it appears that if one begins with the compound α-$Cs_3(HSO_4)_2(H_2PO_4)$ and proceeds to replace some P^{6+} with S^{5+}, the proton that is necessarily also removed for charge balance reasons, derives from the O(11)–O(6) bond between sulfate groups rather from any of the hydrogen bonds in which the phosphate anion participates. As the O(11)–O(6) bond becomes weaker (as a result of the lowered proton occupancy), the constraint, i.e., the hydrogen bond, that breaks the inversion symmetry between neighboring sulfate groups is weakened, and eventually the structure takes on a higher-symmetry configuration. This latter configuration may be expected to be thermodynamically more favorable because of its presumably higher entropy. At this stage, the proton, which was shared between only two oxygen atoms in α-$Cs_3(HSO_4)_2(H_2PO_4)$, becomes shared by four in β-$Cs_3(HSO_4)_2(H_{2-x}(P_{1-x}S_x)O_4)$. The compound containing the maximum phosphorus content is likely unable to crystallize in the $C2/c$ high-symmetry space group, by, for example, replacing the O(11)–O(6) bond in α-$Cs_3(HSO_4)_2(H_2PO_4)$ with one between O(2)–O(11) as this latter distance is 3.717 Å (Fig. 7b) and much too long to accommodate a hydrogen bond. Similarly, the O(5)–O(5′) distance in β-$Cs_3(HSO_4)_2(H_{2-x}(P_{1-x}S_x)O_4)$ is 3.866 Å (Fig. 7a) and too long to permit the formation of a hydrogen bond.

The estimated occupancy of $\frac{1}{4}$ at the H(3) site in β-$Cs_3(HSO_4)_2(H_{2-x}(P_{1-x}S_x)O_4)$ provides for a total of $3\frac{1}{2}$ protons per formula unit and implies that there is, on average, one proton associated with every other O(5)–O(6)–O(5′)–O(6′) group. At present it is unclear whether this low proton occupancy reflects a time-averaged or position-averaged disorder. However, it is noteworthy that the O(5) and O(6) atoms exhibited significantly larger thermal vibrations than the other atoms (Fig. 3) and that Fourier difference maps revealed a small residual electron density peak in their vicinity. These results suggest that there may be some orientational disorder of the SO_4 group that may worthy of further examination by more suitable techniques.

The hydrogen bond networks formed by α-$Cs_3(HSO_4)_2(H_2PO_4)$ and β-$Cs_3(HSO_4)_2(H_{2-x}(P_{1-x}S_x)O_4)$ are, respectively, three-dimensional, and "weakly" three-dimensional in nature. Three-dimensional frameworks, rather than layers, result from the cross-linking of chains at the PO_4 or $(P,S)O_4$ groups because neighboring chains are out of register with one another. That is to say, where one XO_4 unit in a zig-zag chain is in an "up" position, the comparable unit in a neighboring chain is in the "down" position. As a consequence, $PO_4/(P,S)O_4$ groups within one chain form bonds to different neighboring chains (Fig. 7), creating the three-dimensional network observed. These structures differ significantly from that of CsH_2PO_4, in which crosslinking between straight chains of PO_4 groups leads to a two-dimensional layer structure (18). If one considers only the disordered bonds that link $PO_4/(P,S)PO_4$ groups, a one-dimensional chain extending along [100] exists. In β-$Cs_3(HSO_4)_2(H_{2-x}(P_{1-x}S_x)O_4)$ there is one crystallographically distinct bond in this chain, whereas in α-$Cs_3(HSO_4)_2(H_2PO_4)$ there are two. In terms of the distribution of disordered hydrogen bonds, then, these two compounds are quite similar to CsH_2PO_4.

Despite the similarities between the structures of β-$Cs_3(HSO_4)_2(H_{2-x}(P_{1-x}S_x)O_4)$ and α-$Cs_3(HSO_4)_2(H_2PO_4)$, it is noteworthy that their X-ray powder diffraction patterns differ to an extent that makes it possible to readily distinguish the two. The experimental and calculated patterns are compared in Fig. 8. The clear differences between the patterns and between the respective IR and Raman spectra (Fig. 1) also demonstrate that these two compounds are indeed distinct phases.

Optical Spectroscopy

The low symmetry of β-$Cs_3(HSO_4)_2(H_{2-x}(P_{1-x}S_x)O_4)$ and α-$Cs_3(HSO_4)_2(H_2PO_4)$, as well as the existence of multiple, crystallographically independent X atoms, renders a complete group factor analysis of these compounds not only difficult, but also somewhat meaningless. To make a qualitative assignment of Raman peaks to vibrational modes, most of which are tied to XO_4 group vibrations, we examine the modes and frequencies observed for H_nXO_4 anions (21). The ideal, five-atom PO_4 or SO_4 tetrahedral

group exhibits T_d symmetry. Thus, there are nine vibrational modes, only four of which are independent: $\nu_1(a_1) = XO_4$ symmetric stretch; $\nu_2(e \times 2) =$ O–X–O bend; $\nu_3(f_2 \times 3) = XO_4$ asymmetric stretch; and $\nu_4(f_2 \times 3) =$ O–X–O bend. The influence of the addition of protons to the anion can be understood through a two-step process. First, in HXO_4, one of the oxygen atoms is replaced with a hydroxyl group with point mass. This reduces the symmetry from T_d to C_{3v}, and eliminates degeneracies such that there are six rather than four independent vibrational modes. Second, the vibrations associated with the hydroxyl group are considered. There should be three such modes: O–H stretching, X–O–H in-plane bending, and X–O–H out-of-plane bending (or torsion). Similarly, the H_2XO_4 ion (or molecule) can be considered a group with C_{2v} symmetry and therefore nine independent internal modes. In addition, there are six modes associated with the hydroxyl groups, as the $X(OH)_2$ stretching and bending modes may now be either symmetric or asymmetric. The case of H_3XO_4, which ideally displays C_{3v} symmetry, is similar to that of HXO_4; however, there are additional O–H modes. Literature values for the frequencies of each of these vibrations in H_nXO_4 groups are listed in Table 7.

To apply these concepts to the Raman spectra of β-$Cs_3(HSO_4)_2(H_{2-x}(P_{1-x}S_x)O_4)$ and α-$Cs_3(HSO_4)_2(H_2PO_4)$, it is necessary to first identify the H_nXO_4 groups present within each structure. Ignoring the effect of protons bonded to acceptor oxygen atoms or to mixed acceptor/donor atoms, the former has one $(P, S)O_4$ group (free of protons) and one HSO_4 group (Table 4). The compound α-$Cs_3(HSO_4)_2(H_2PO_4)$, in contrast, has one H_2PO_4 group, one HSO_4 group, and one SO_4 group (10). Both compounds exhibit Raman peaks in the regions 410–500, 580–635, 820–1100, and 1120–1245 cm^{-1} (Table 8). Those peaks in β-$Cs_3(HSO_4)_2(H_{2-x}(P_{1-x}S_x)O_4)$ have an average full width half-maximum of 27 cm^{-1}, whereas those in α-$Cs_3(HSO_4)_2(H_2PO_4)$ have a value of 15 cm^{-1}. Moreover, there are a greater number of peaks in the spectrum obtained from α-$Cs_3(HSO_4)_2(H_2PO_4)$ than from β-$Cs_3(HSO_4)_2(H_{2-x}(P_{1-x}S_x)O_4)$. Both observations are consistent with the lower symmetry, greater number of crystallographically distinct X atoms, and higher general state of order in the former than in the latter. While the resolution of the IR spectra is not as good as that of the Raman spectra, it is noteworthy that there is one relatively sharp peak at 725 cm^{-1} in the IR spectra of both α-$Cs_3(HSO_4)_2(H_2PO_4)$ and β-$Cs_3(HSO_4)_2(H_{2-x}(P_{1-x}S_x)O_4)$ that does not appear in the Raman data.

The Raman peaks obtained in the low-frequency regions of the spectra (< 650 cm^{-1}) most likely correspond to internal bending modes of the H_nXO_4 groups. With the exception of the appearance of extra peaks in the spectrum of

TABLE 7
Vibrational Modes and Frequencies of H_nXO_4 Anions (cm^{-1})

Mode: Ref.:	$T_d XO_4$	SO_4^{2-} (a)[a]	PO_4^{3-} (a)	C_{3v} HXO_4	HSO_4^- (b)	HPO_4^{2-} (c)	C_{3v} H_3XO_4	H_3PO_4 (d)	C_{2v} H_2XO_4	H_2SO_4 (b)	$H_2PO_4^-$ (c)
Bend	E (×2) $\delta_d(OXO)$ (ν_2)	451	358	E (×2) $\delta_{as}(OXO)$	440	~390	E (×2) $\delta_{as}(OHXOH)$	500	A_1 $\delta(OXO)$	563	380[b]
									A_2 $\rho_t(XO_2)$	392	
Bend	F_2 (×3) $\delta_d(OXO)$ (ν_4)	613	500	A_1 $\delta_s(OXO)$	608	~530	A_1 $\delta_s(OHXOH)$	500	A_1 $\delta(OHXOH)$	392	
				E (×2) $\rho_r(XO_3)$	n/a	~530	E (×2) $\rho_r(X(OH)_3)$	376	B_1 $\rho_r(XO_2)$	563	514[b]
									B_2 $\rho_w(XO_2)$	422	
Stretch	A_1 $\nu_s(XO)$ (ν_1)	980	970	A_1 $\nu(XOH)$	902	850	A_1 $\nu(XO)$	890	A_1 $\nu(XOH)$	910	874
Stretch	F_2 (×3) $\nu_{as}(XO)$ (ν_3)	1104	1080	A_1 $\nu_s(XO_3)$	1036	987	A_1 $\nu_s(XOH)$	1178	A_1 $\nu(XO)$	1194	1074
				E (×2) $\nu_{as}(XO_3)$	1195	1080	E (×2) $\nu_{as}(XOH)$	1006	B_1 $\nu(XO)$	1368	1150
									B_2 $\nu(XOH)$	973	940

[a] Sources: (a) Irish and Ozeki (22); (b) Gillespie and Robinson (23); (c) Preston and Adams (24); (d) Rudolph and Steger (25).
[b] Simply designated "bending modes" without specification of the motion.

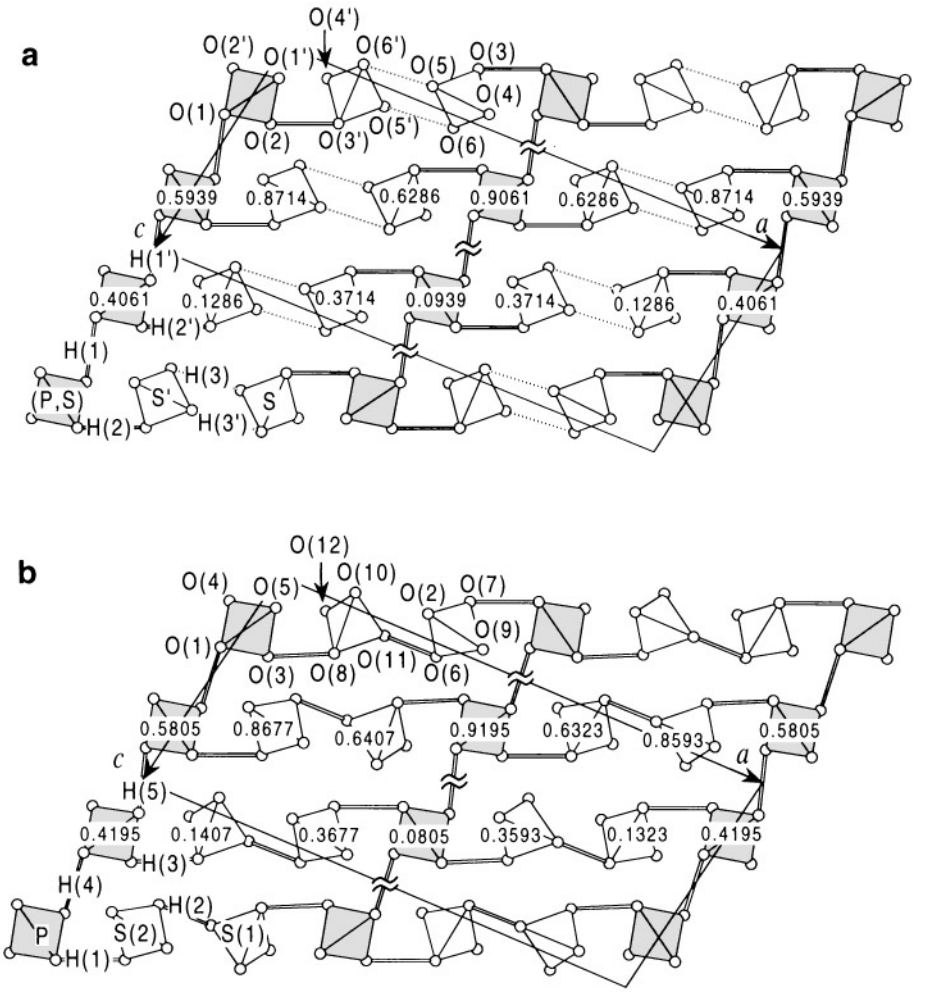

FIG. 7. Structures of β-$Cs_3(HSO_4)_2(H_{2-x}(P_{1-x}S_x)O_4)$ (a, c) and of α-$CS_3(HSO_4)_2(H_2PO_4)$ (b, d) shown in projection on (010). The elevations of the central X atoms are as given in (a) and (b). For clarity protons have been omitted from the figures, but bonds between hydrogen-bonded oxygen atoms are shown. Wavy lines in (a) and (c) that break hydrogen bonds indicate that one of the oxygen atoms in the hydrogen-bonded pair is not shown in the figure. For clarity, these bonds are omitted in (c) and (d).

α-$Cs_3(HSO_4)_2(H_2PO_4)$ at 475, 497, and 628 cm^{-1}, the spectra of the two materials are almost identical in this range. The peaks obtained in the region from 820 to 1100 cm^{-1} most likely correspond to H_nXO_4 stretching modes. In the case of α-$Cs_3(HSO_4)_2(H_2PO_4)$ the stretching modes appear to be further distinguished into those with frequencies between 810 and 920 cm^{-1} and those with frequencies between 970 and 1100 cm^{-1}. The three low-frequency stretches are interpreted to correspond to X–OH stretches, in particular, to the S–OH stretch of the HSO_4 ion and the symmetric and antisymmetric P–$(OH)_2$ stretches of the H_2PO_4 ion. The higher-frequency stretching modes are believed to reflect modes involving XO_n, for example, the symmetric and antisymmetric P–O_2 stretches of the H_2PO_4 ion and the S–O_3 stretch of the HSO_4 ion. The peaks in the 820 to 1100 cm^{-1} region of the β-$Cs_3(HSO_4)_2(H_{2-x}(P_{1-x}S_x)O_4)$ spectrum are not nearly as well resolved as those of the α-$Cs_3(HSO_4)_2(H_2PO_4)$ spectrum. This likely results from the two types of disorder noted in the structure of β-$Cs_3(HSO_4)_2(H_{2-x}(P_{1-x}S_x)O_4)$. First, the existence of both P and S on the same site leads to a smearing out of the X–O_4 stretching frequencies of the $(P,S)O_4$ ion. More importantly, the partial occupancy at the H(3) site results in sulfate groups that are in some cases HSO_4 ions, as assumed above, and in some cases H_2SO_4 ions. Thus, there is no clear distinction between sulfate stretching modes that involve singly protonated and doubly protonated anion groups. This is compounded by the fact that the oxygen atoms about the sulfur have, as discussed above, large thermal vibrations, indicating that they reside in shallow and possibly severely anharmonic potential wells or that the sulfate group itself may even undergo librations.

The Raman peaks obtained in the region from 1120 to 1245 cm^{-1} are presumed to result primarily from X–O–H

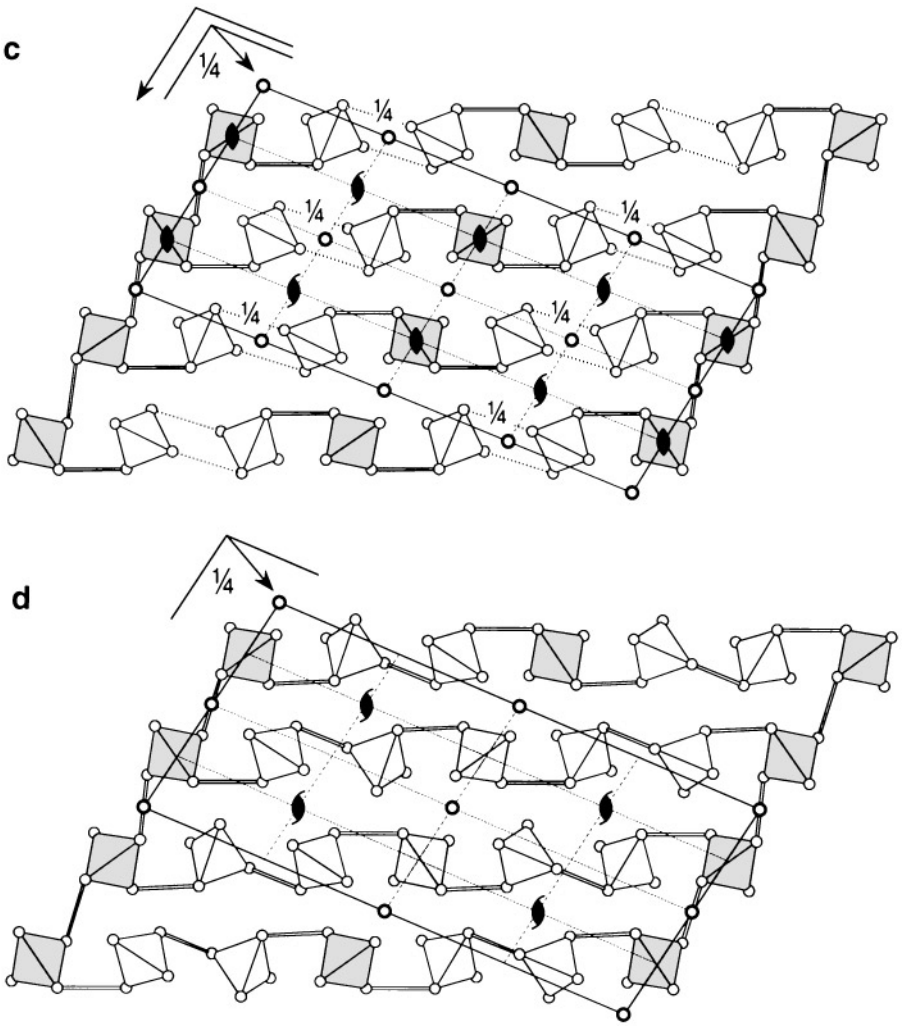

FIG. 7—*Continued*

in-plane bending modes, although there may be some contribution from X–O and X–OH stretching modes. In this region of the spectrum the peaks from β-$Cs_3(HSO_4)_2(H_{2-x}(P_{1-x}S_x)O_4)$ are particularly broad relative to those of α-$Cs_3(HSO_4)_2(H_2PO_4)$, reflecting, again, the disorder in the structure of β-$Cs_3(HSO_4)_2(H_{2-x}(P_{1-x}S_x)O_4)$ in the vicinity of the proton sites. The IR peaks observed in both β-$Cs_3(HSO_4)_2(H_{2-x}(P_{1-x}S_x)O_4)$ and α-$Cs_3(HSO_4)_2(H_2PO_4)$ at $\sim 725\,cm^{-1}$ likely corresponds to an X–O–H out-of-plane bending mode. Marchon and Novak (26) have made such an assignment for two peaks observed in the IR spectrum of CsH_2PO_4 at 966 and $872\,cm^{-1}$ that were similarly Raman inactive. The high-frequency peaks noted in both the IR and Raman Spectra of both compounds (at $\sim$2900, 2300, and $1700\,cm^{-1}$), have also been observed in the spectrum of CsH_2PO_4 (at 2700, 2300, and $1700\,cm^{-1}$) and are interpreted as OH stretching modes in Fermi resonance with combinations of OH bending vibrations (26).

Proton Conductivity and Phase Transitions

Proton transport in "superprotonic" materials such as $CsHSO_4$-I is generally understood to take place via a two-step process (27). The first step involves a proton jump from one XO_4 group to the next, and the second, the relaxation and reorientation of XO_4 groups into positions that are favorable for step 1. Such a diffusion process is sometimes known as a "structure" or "Grotthuss" mechanism. The signatures of dynamic XO_4 group reorientation and proton mobility in diffraction experiments are partially occupied oxygen and proton sites. Precisely these features, in particular, a partially occupied proton site and large O(5) and O(6) thermal vibrations, have been observed for β-$Cs_3(HSO_4)_2(H_{2-x}(P_{1-x}S_x)O_4)$, and they undoubtedly explain the unusually high proton conductivity of this material at ambient temperatures (5). In addition, the compound undergoes a superprotonic transition at 125°C, exhibiting an increase

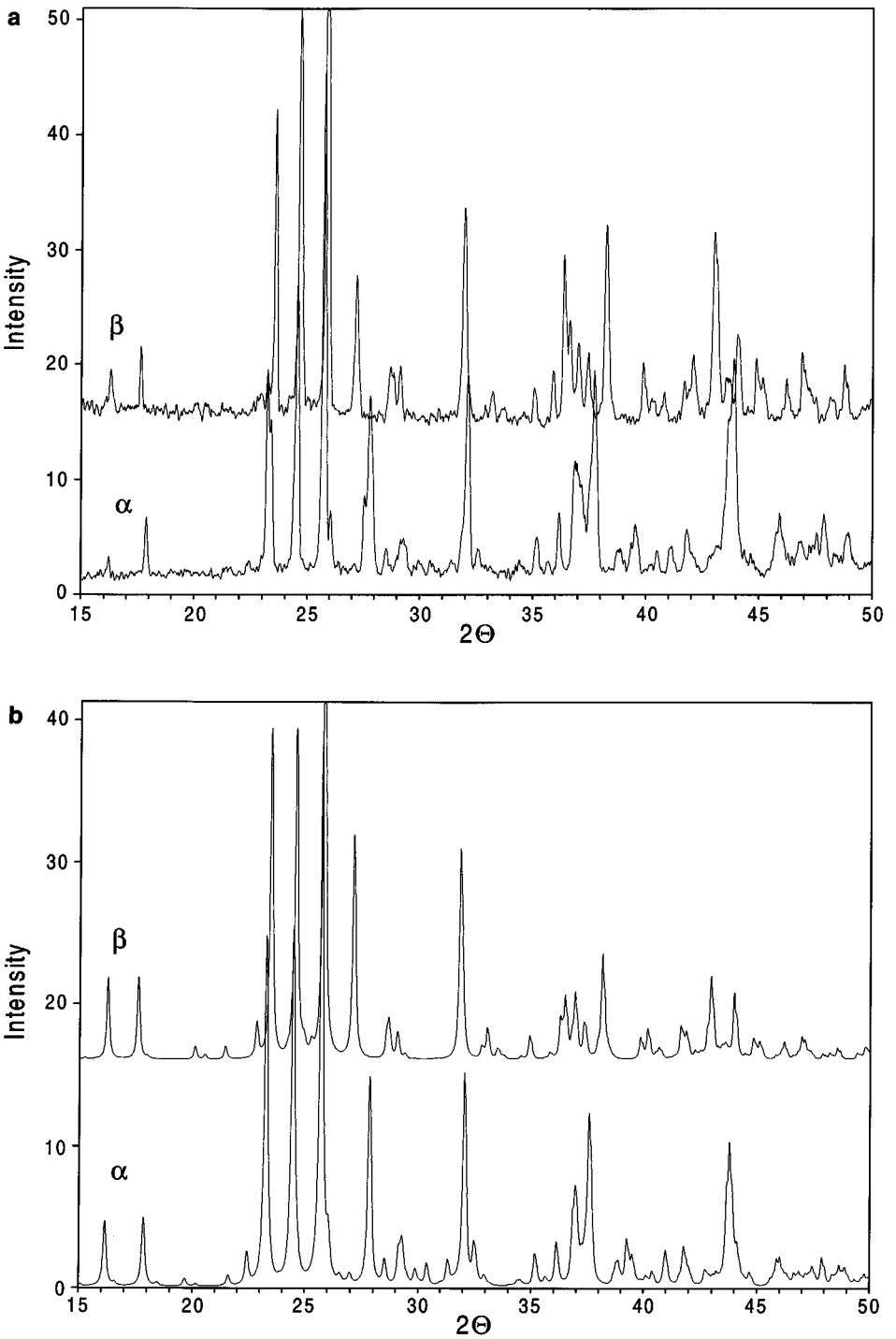

FIG. 8. Comparison of the X-ray powder diffraction patters of β-$Cs_3(HSO_4)_2(H_{2-x}(P_{1-x}S_x)O_4)$ and α-$CS_3(HSO_4)_2(H_2PO_4)$. (a) Experimentally obtained. (b) Calculated.

in conductivity of more than two orders of magnitude. The transition, similar to that in $CsHSO_4$, is important in that it demonstrates, together with our earlier observation of a transition in α-$Cs_3(HSO_4)_2(H_2PO_4)$, that phosphorus has no negative impact on superprotonic transitions. The alkali dihydrogen phosphate compounds, in contrast, undergo thermal decomposition at elevated temperatures, before the onset of inherently high conductivity (28). In Haile *et al.* (10) we provide a possible explanation for the differences in behavior of the MH_2PO_4 compounds and the

TABLE 8
Positions and Relative Intensities of Peaks in the Raman Spectra of β-$Cs_3(HSO_4)_2(H_{2-x}(P_{1-x}S_x)O_4)$ and α-$Cs_3(HSO_4)_2(H_2PO_4)$

β-$Cs_3(HSO_4)_2(H_{2-x}(P_{1-x}S_x)O_4)$		α-$Cs_3(HSO_4)_2(H_2PO_4)$		
Wavenumber (cm^{-1})	Intensity	Wavenumber (cm^{-1})	Intensity	Qualitative Assignment
360	11	349	3	
426	58	418	34	
		431	31	
445	37	443	14	
		475	9	Bending modes
		497	4	
521	11	523	1	
590	54	587	58	
614	13	602	4	
		628	6	
832	5	826	18	
864	14	854	18	*X*–OH
910	47	901	19	stretching modes
947	42			
969	100	979	29	
993	57	993	63	*X*–O
		1006	20	stretching modes
1039	56	1026	32	
1083	11	1048	100	
1126	12	1130	5	
1164	18	1186	12	*X*–O–H in-plane
1205	18	1219	16	bending modes
1243	1	1244	6	

sulfate-containing compounds on the basis of the hydrogen bond network. Essentially, it is proposed that the presence of oxygen atoms with different hydrogen bond environments (at room temperature) is a key prerequisite for superprotonic behavior at elevated temperatures. In this model, entropic considerations that favor chemically equivalent bonds drive a transition to a disordered state, which, in turn, leads to high conductivity. Because MH_2PO_4 compounds have saturated H_2PO_4 groups, all oxygen atoms participate in hydrogen bond formation at room temperature, and there is no driving force for a structural transition.

ACKNOWLEDGMENTS

This work was supported in part by the National Science Foundation through a National Young Investigator Award, by Battelle National Laboratories, and by the Electric Power Research Institute. The authors thank Scott Kuehner of the University of Washington for assistance with the electron microprobe analyses, and Dr. Wim Klooster of Brookhaven National Laboratories for providing the results of a preliminary refinement of neutron diffraction data. Alex Katz of the California Institute of Technology kindly collected IR and Raman spectra.

REFERENCES

1. A. I. Baranov, L. A. Shuvalov, and N. M. Shchagina, *JETP Lett*. **36,** 459 (1982).
2. A. Pawlowski, Cz. Pawlaczyk, and B. Hilczer, *Solid State Ionics* **44,** 17 (1990).
3. B. V. Merinov, A. I. Baranov, L. A. Shuvalov, and N. M. Shchagina, *Sov. Phys. Cryst*. **36,** 321 (1991).
4. S. Haile, G. Lentz, K.-D. Kreuer, and J. Maier, *Solid State Ionics* **77,** 128 (1995).
5. S. M. Haile, P. M. Calkins, and D. Boysen, *Solid State Ionics* **97,** 145 (1997).
6. F. Schamber, N. Wodke, and J. McCarthy, "ZAF Matrix Correction Procedure for Bulk Samples: Operation and Program Description," Publication TN-2120. Tracor Northern, Middleton, WI, 1981.
7. G. D. Christian, "Analytical Chemistry," 5th ed. Wiley, New York, 1994.
8. S. M. Haile and P. M. Calkins, accepted, *J. Solid State Chem.*
9. P. M. Calkins, M.S. thesis, University of Washington, 1996.
10. S. M. Haile, K.-D. Kreuer, and J. Maier, *Acta Crystallogr. Sect. B* **53,** 680 (1995).
11. W. T. Klooster and S. M. Haile, under preparation.
12. D. T. Cromer and J. T. Waber, "International Tables for X-ray Crystallography," Vol. IV, Table 2.2A, pp. 128–134. Kynoch Press, Birmingham, 1974. (Present distributor Kluwer Academic Publishers, Dordrecht.)
13. G. M. Sheldrick, *in* "Crystallographic Computing 3" (G. M. Sheldrick, C. Krüger, and R. Goddard, Eds.), pp. 175–189. Oxford Univ. Press, Oxfordshire, 1985.
14. G. M. Sheldrick, *in* "Crystallographic Computing 6" (H. D. Flack, L. Parkanyi, and K. Simon, Eds.), pp. 100–110. Oxford Univ. Press, Oxfordshire, 1993.
15. R. D. Shannon and C. T. Prewitt, *Acta Crystallogr. Sect. B* **25,** 925 (1969).
16. M. Ichikawa, *Acta Crystallogr. Sect. B* **43,** 23 (1986).
17. M. Ichikawa, *Acta Crystallogr. Sect. B* **34,** 2074 (1978).
18. H. Matsunaga, K. Itoh, and E. Nakamura, *J. Phys. Soc. Japan* **48,** 2011 (1980).
19. Y. Noda, S. Uchiyama, K. Kafuku, H. Kasatani, and H. Terauchi, *J. Phys. Soc. Japan* **59,** 2804 (1990).
20. A. V. Belushkin, W. I. F. David, R. M. Ibberson, and L. Shuvalov, *Acta Crystallogr. Sect. B* **47,** 161 (1991).
21. K. Nakamoto, "Infrared Spectra of Inorganic and Coordination Compounds." Wiley, New York, 1963.
22. D. E. Irish and T. Ozeki, *in* "Chemical Analysis" (J. G. Gasselli and B. J. Bulkin, Eds.), Vol. 114, Chap 4. Wiley, New York, 1991.
23. R. J. Gillespie and E. A. Robinson, *Can. J. Chem*. **40,** 644 (1962).
24. C. M. Preston and W. A. Adams, *J. Phys. Chem*. **83,** 814 (1979).
25. Von W. Rudolph and W. E. Steger, *Z. Phys. Chem*. **172,** 49 (1991).
26. B. Marchon and A. Novak, *J. Chem. Phys*. **78,** 2105 (1983).
27. K.-D. Kreuer, *Chem. Mater*. **8,** 610 (1996).
28. K.-S. Lee, *J. Phys. Chem. Solids* **57,** 333 (1996).